

SCIENTIFIC REPORTS



OPEN

CVD graphene as an electrochemical sensing platform for simultaneous detection of biomolecules

Xiaodan Wang¹, Delan Gao¹, Mingji Li¹, Hongji Li², Cuiping Li¹, Xiaoguo Wu¹ & Baohe Yang¹

The development of electrochemical biosensors for the simultaneous detection of ascorbic acid (AA), dopamine (DA), uric acid (UA), tryptophan (Trp), and nitrite (NO₂⁻) in human serum is reported in this work. Free-standing graphene nanosheets were fabricated on Ta wire using the chemical vapor deposition (CVD) method. CVD graphene, which here served as a sensing platform, provided a highly sensitive and selective option, with detection limits of AA, DA, UA, Trp, and NO₂⁻ of 1.58, 0.06, 0.09, 0.10, and 6.45 μM (S/N = 3), respectively. The high selectivity of the electrode is here explained by a relationship between the bandgap energy of analyte and the Fermi level of graphene. The high sensitivity in the oxidation current was determined by analyzing the influence of the high surface area and chemical structure of free-standing graphene nanosheets on analyte adsorption capacity. This finding strongly indicates that the CVD graphene electrode can be used as a biosensor to detect five analytes in human serum.

Electrochemical biosensors that have high sensitivity have found widespread use in clinical diagnosis^{1–4}. Human body fluids contain electrolytes, including a wide variety of electroactive materials, including biological, organic, and inorganic electrolytes. L-ascorbic acid (AA), dopamine (DA), uric acid (UA), tryptophan (Trp), and nitrite (NO₂⁻) are found in body fluids. Scurvy is caused by a deficiency of AA⁵, and abnormal DA transmission has been implicated in Huntington's disease and neuroendocrine disorders⁶. Abnormalities in UA levels indicate symptoms of gout, hyperuricemia, and leukemia^{7, 8}; Trp is an essential amino acid and that is a serotonin precursor, Parkinson's disease linked to Trp⁹; NO₂⁻ is an important precursor in the formation of N-nitrosamines, many of which have been shown to be potent carcinogens in humans^{10–12}. AA, DA, UA, Trp, and NO₂⁻ usually coexist in body fluids^{13, 14}. Thus, the development of sensors for the simultaneous detection of AA, DA, UA, Trp, and NO₂⁻ with sensitivity and selectivity is highly important to the investigation of their physiological functions and to diagnostic and analytical applications.

One major problem troubling the development of such sensors is that AA, DA, UA, Trp, and NO₂⁻ all undergo oxidation at the closed potentials of conventional electrodes. This mutual interference from each other should be expected and must be taken into account. In addition, conventional electrodes have a pronounced fouling effect, which can result in poor selectivity and reproducibility. To overcome these obstacles, so far, various materials have been used to modify conventional electrodes for the simultaneous detection of AA, DA, and UA^{15–17}; of UA and Trp¹⁸; of Trp and NO₂⁻, of DA, UA and Trp^{19, 20}; of AA, DA, UA, and Trp^{21, 22}; and of AA, DA, UA, and NO₂⁻. Unfortunately, there have been no reports that the simultaneous determination of all five. Many reported methods of simultaneous detection (for two or three or four of these electroactive compounds) are complicated, expensive, unstable, and have sensing layers that detached from the basic electrode easily.

Graphene is one of the most commonly used materials in electrodes, in which it serves as a sensitive film. The graphene materials include graphene oxide (GO), reduced graphene oxide (rGO), and chemical vapor deposition (CVD) graphene. Of these, GO and rGO are the most commonly used in electrochemical sensors^{23–27}. According

¹Tianjin Key Laboratory of Film Electronic and Communicate Devices, School of Electrical and Electronic Engineering, Tianjin University of Technology, Tianjin, 300384, P.R. China. ²Tianjin Key Laboratory of Organic Solar Cells and Photochemical Conversion, School of Chemistry and Chemical Engineering, Tianjin University of Technology, Tianjin, 300384, P.R. China. Correspondence and requests for materials should be addressed to M.L. (email: limingji@163.com) or H.L. (email: hongjili@yeah.net)

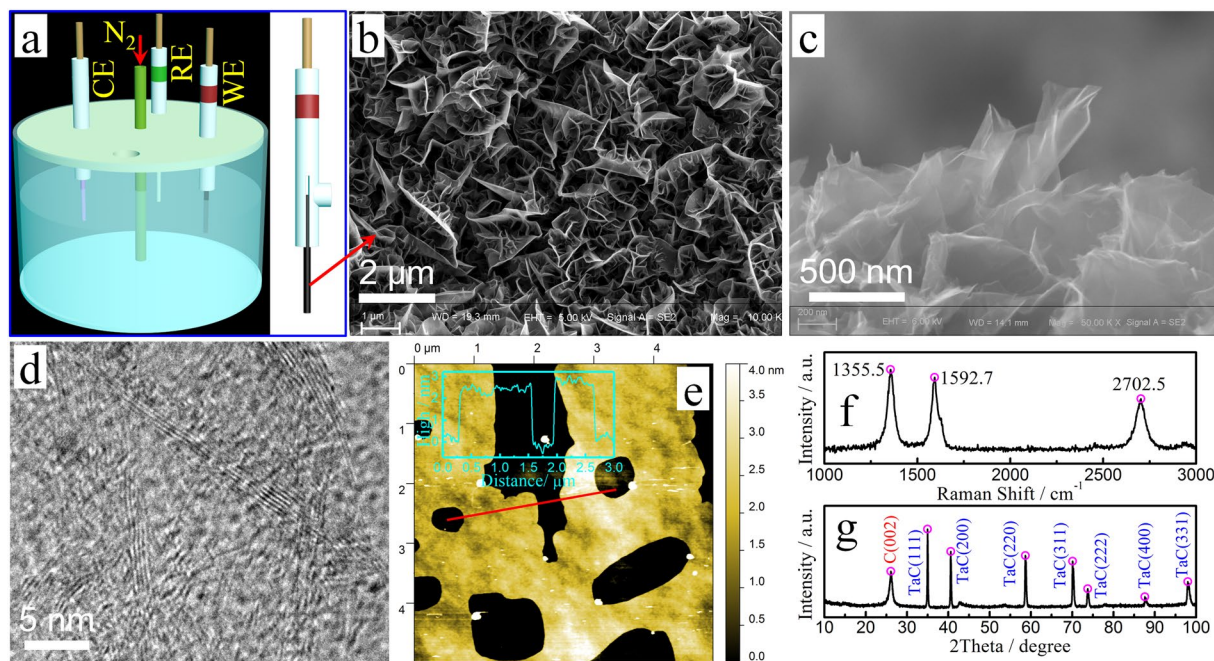


Figure 1. (a) Schematic diagram of electrolytic cell and electrodes. Dissolved oxygen was removed by passing N_2 into the electrolytic cell. Counter electrode (CE), reference electrode (RE), and working electrode (WE) are platinum sheet, saturated calomel electrode, and graphene/Ta wire, respectively. (b) Top-view and (c) cross-sectional SEM images of graphene nanosheets. (d) High-resolution TEM image of graphene nanosheets. (e) AFM image of graphene nanosheets. (e) Inset showing height profile along line. (f) Raman spectrum and (g) XRD pattern of graphene/Ta wire.

to the references, the GO composite-modified-electrodes were detected simultaneously with the DA and 5-hydroxytryptamine²⁸, DA and UA²⁹, guanine and adenine³⁰, AA, DA, and UA^{31,32}, AA, DA, UA, and folic acid³³, and l-tyrosine and l-tyrosine³⁴. However, these graphene-based materials use of drip coating, electrodeposition, and screen printing method, these graphene based-materials are modified to the basis electrodes. Weak adhesion between the sensitive film and the based electrode can shorten the life of the sensitive layer. They also require special storage conditions. CVD graphene has higher electrical conductivity and fewer defects than graphene prepared using wet-chemical methods³⁵. CVD graphene is grown directly on the conductor, and the strong binding between the two prevents them separating from each other^{36,37}. These give the electrodes strong stability and long life. The CVD graphene-based sensor has been used to detect levodopa³⁸ and glucose^{39,40}. Further increases in the surface area of graphene electrodes have been found to enhance the adsorption capacity of graphene layer for the analyte^{41,42}, thereby increasing the sensitivity of the graphene electrode. To achieve this, the vertical growth of graphene must be fostered to form a graphene wall on a metal substrate. Moreover, these graphene walls would ideally be highly dense, and the high edge density increases the charge storage ability⁴³, thereby increasing adsorption and accelerating the electron transfer rate. More importantly, free-standing graphene walls are regularly exposed to different edge structures, which indicates the presence of different band-gap energy levels on graphene layer⁴⁴. This renders the electronic transition process different from that of other graphene⁴⁵, then the sensitive layer may have a better potential selectivity. Recently, a method of directly synthesizing graphene electrodes using CVD has been developed. This made the production of high-quality graphene with vertically oriented features possible⁴⁶.

Based on these above considerations, a biosensing electrode with CVD graphene as sensitive layer was here developed, and Ta wire served as the basis electrode. The present work focuses on evaluating the simultaneous detection of AA, DA, UA, Trp, and NO_2^- , and response mechanism of this graphene designed for the simultaneous detection of multiple analytes is evaluated.

Results

Characterization of graphene/Ta wire electrodes. Figure 1a shows the three-electrode testing system with the graphene/Ta wire as the sensing electrode. Figure 1b and c clearly indicate that graphene layers with pores between the graphene sheets formed an open network. The graphene sheets were thin and transparent, and the thinner sheet was divided from the surface of the nanosheet. The graphene layer contained many curved nanosheets with vertical growth trends. Network structures of graphene nanosheets provide more channels between the graphene sheets to facilitate the entrance of electrolyte ions or electrons into the inter-space. The effective area of graphene layers calculated using electrochemical kinetics is 2.24 cm^2 (Fig. S1), which is ten times the actual area (0.2262 cm^2) of graphene/Ta wire electrode. The thickness of graphene nanosheets can be confirmed using high-resolution transmission electron microscopy (TEM) (Fig. 1d) and atomic force microscopy

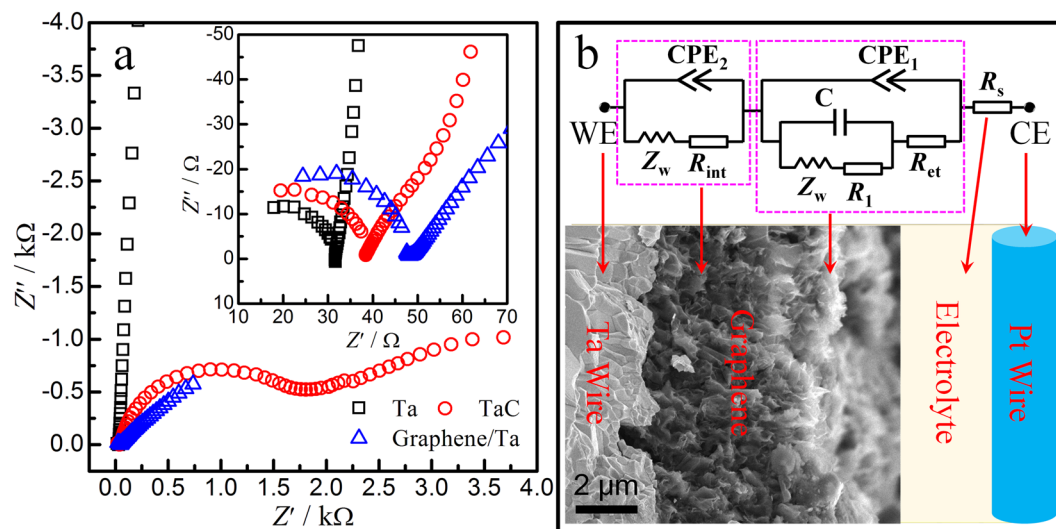


Figure 2. (a) Impedance spectra of the Ta wire, TaC/Ta wire, and graphene/Ta wires in 0.1 KCl containing 5 mM $\text{K}_3\text{Fe}(\text{CN})_6$ and 5 mM $\text{K}_4\text{Fe}(\text{CN})_6$.

(AFM) (Fig. 1e) images. The thickness of these graphene sheets ranged from 0.34 nm to 3 nm, corresponding to stacking of approximately 1–10 layers of the monoatomic graphene sheets. The conductivity of graphene affects the sensitivity of the sensing electrode. The conductivity of multi-layer graphene is lower than that of single-layer graphene. Compared with the low-layer graphene prepared by the liquid-phase oxidation method, the vertical multi-layer graphene sheets prepared using the CVD method have high orientation, low contact resistance (between the Ta wire and graphene layer), and less oxygen-containing groups, which impart high electrical properties to the prepared graphene/Ta wire. Of course, if we can prepare a graphene electrode with vertically arranged single-layer graphene sheets, then the sensitivity of the graphene electrode will be higher than the current graphene/Ta wire.

The Raman spectrum of graphene layer is shown in Fig. 1f. The spectrum feature include a D band at approximately 1355.5 cm^{-1} , G band at around 1592.7 cm^{-1} , and 2D band at approximately 2702.5 cm^{-1} . The D band is a characteristic feature, indicating defects. It can be caused by excitation of the edges of graphene sheets and their random orientation^{47,48}. The G band shows sp^2 vibrations in the graphitic plane, which confirms the presence of graphene sheets. Intense, well-defined 2D bands with a narrow width of full width at half maximum is peculiar for few layer graphene. The X-ray diffraction (XRD) pattern of the graphene/Ta wire is shown in Fig. 1g. A sharp peak at about $2\theta = 26^\circ$ corresponding to the (002) reflection of graphite (JCPDS 75–1621) was observed with interlayer space (d-spacing) of 0.34 nm, indicating the graphene layer formed on Ta wire. In addition, the TaC phases were observed, which indicated that the carbon atoms first dissolved into the interior of Ta which formed the TaC transition layer and then formed graphene nanosheets through further deposition of carbon atoms⁴⁶.

Electrochemical behaviors of graphene electrode. Figure 2a compares the Nyquist plots of pure Ta wire, TaC/Ta wire, and graphene/Ta wire in 0.1 M KCl solution containing 5.0 mM $\text{K}_3[\text{Fe}(\text{CN})_6]$ and 5.0 mM $\text{K}_4[\text{Fe}(\text{CN})_6]$, respectively. For the TaC/Ta wire, the Nyquist plot consisted of two semicircles in high- and medium-frequency regions followed by an inclined line in low-frequency region. For the graphene/Ta wire, the Nyquist plots consisted of a semicircle in high-frequency region followed by an inclined line in a medium-low-frequency region. According to the Randles-type circuit in Fig. 2b, the series resistance (R_s) is created by the electrolyte. The semicircle indicates the charge-transfer resistance (R_{ct}) at the external graphene/electrolyte interface; the interface resistance (R_{int}) is contributed from the bottom graphene layer. As shown, the diameter of the semicircle for the TaC/Ta wire ($R_{ct} = 200\ \Omega\ \text{cm}^2$) is much larger than that of the graphene/Ta wire ($R_{ct} = 37.2\ \Omega\ \text{cm}^2$), indicating the graphene/Ta wire electrode exhibited better charge transfer performance than the TaC/Ta wire and had excellent conductivity.

The individual electrochemical response of these analytes needs to be studied before the sensitivity of graphene/Ta wire electrodes toward the simultaneous detection of AA, DA, UA, Trp, and NO_2^- can be evaluated. The signal responses of graphene/Ta wire electrode for the oxidation of individual AA, DA, UA, Trp, and NO_2^- were investigated by differential pulse voltammetry (DPV) in 0.1 M PBS solution (pH 7.0) by varying their concentrations, as shown in Fig. 3a. The oxidation potentials from highest to lowest were NO_2^- (0.725 V) > Trp (0.58 V) > UA (0.25 V) > DA (0.115 V) > AA (−0.09 V), which shown in Fig. S2. The oxidation potential is generally governed by electron transfer from the analyte to the sensing electrode and hole transfer from the analyte to the counter electrode⁴⁹. The graphene/Ta wire for use as a sensing electrode, the oxidation potential is dominated by both the difference in energy between the Fermi level of graphene ($E_F \approx -4.6\text{ eV}$)⁵⁰ and the highest occupied molecular orbital (HOMO) of analytes, and energy gaps between the HOMO and lowest unoccupied molecular orbital (LUMO) of the analytes. HOMO and LUMO energies approximately represent the ability of molecules to donate and accept electrons⁵¹. H. Y. *et al.*⁴⁹, reported that the oxidation potential increases with the

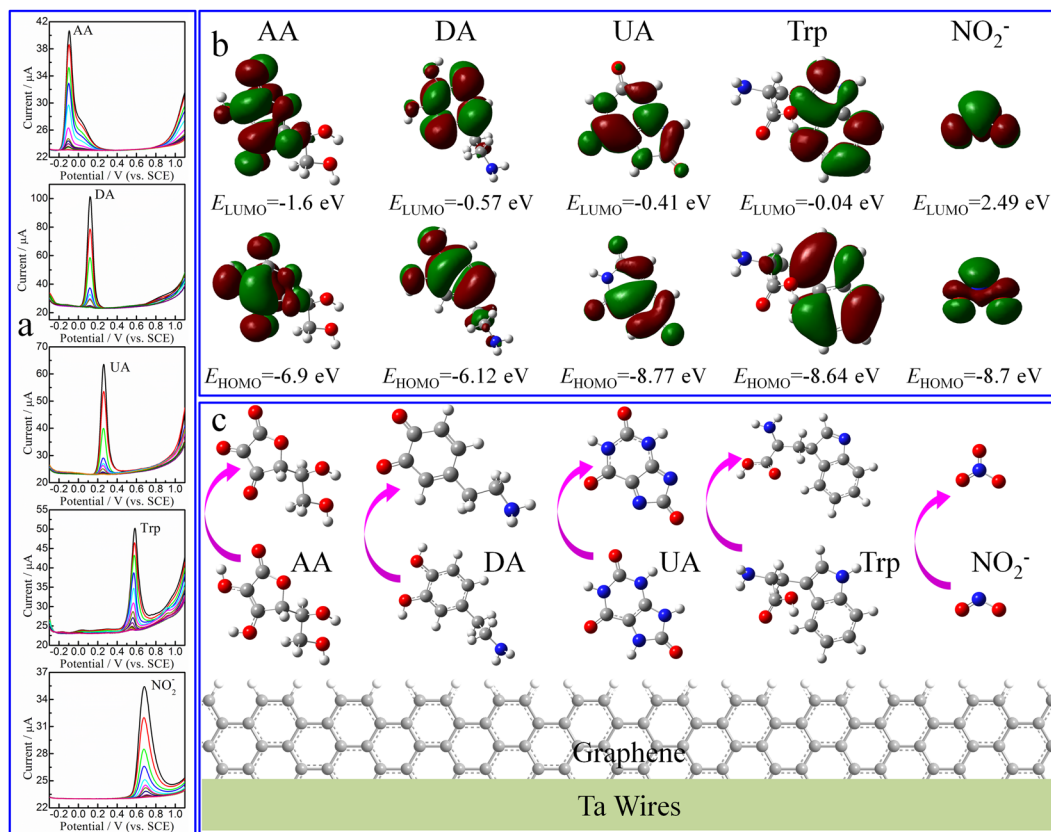


Figure 3. (a) DPVs of graphene/Ta wire electrode in pH 7.0 PBS by varying the concentrations of AA, DA, UA, Trp, and NO₂⁻. (b) Frontier molecular orbitals of AA, DA, UA, Trp, and NO₂⁻. (c) Schematic representation of the biosensing mechanism of the graphene/Ta wire electrode.

increase of LUMO-HOMO energy gap. In this study, molecules and MO orbitals were prepared using GaussView 5.0 and all the calculations were performed using Gaussian V9.5. Moreover, all the molecules were fully optimized using the density functional theory (DFT)/B3LYP method with 6–31 G basis sets in water. The MO data was calculated at the B3LYP/6-311++G (d, p) level for AA and DA, while that of UA, Trp, and NO₂⁻ was at the RHF/AM1 level. Frontier molecular orbital analyses of the HOMO and the LUMO are summarized in Fig. 3b. The LUMO-HOMO energy gaps were, from highest to lowest, NO₂⁻ (11.19 eV) > Trp (8.6 eV) > UA (8.36 eV) > DA (5.55 eV) > AA (5.33 eV). The E_{F} (of graphene)-HOMO (of analyte) values decreases in the order UA (4.17) > NO₂⁻ (4.1) > Trp (4.04 eV) > AA (2.3) > DA (1.52). The effect of pH and solvent on the peak potential of the analyte is relatively large⁵². Dissociation constant ($\text{p}K_{\text{a}1}$) values of AA, DA, UA, Trp, and NO₂⁻ are 4.17, 10.6, 5.75, 2.38 ($\text{p}I = 5.89$), and 3.29. The DA molecules did not dissociate into anions in pH 7.0 PBS, which further increased the oxidation potential of DA. Corresponding to the difference in the dipole moment, the HOMO and LUMO of Trp are localized on the indole ring, the LUMO of NO₂⁻ was highly asymmetrical, and the electron in the LUMO orbitals of Trp and NO₂⁻ was not delocalized onto the graphene layer, thus leading to more positive oxidation potentials of Trp and NO₂⁻ than those of AA, DA, and UA. Considering these factors, the order of electrocatalytic potentials was found to be NO₂⁻ > UA > Trp > AA > DA.

The sensing mechanism of the graphene/Ta wire is shown in Fig. 3c. The anodic peaks correspond to the oxidation of hydroxyl groups to carbonyl groups of the furan ring in AA, oxidation of catechol to o-quinone in DA, oxidation of bridging double bonds to hydroxyl groups in UA, oxidation of the phenyl ring in Trp, and oxidation of the NO₂⁻ to NO₃⁻. The oxidation peak current is determined using the sum of the electron flow to the graphene and the hole flow to the Pt electrode. The oxidation current is affected by the adsorption strength between the graphene and the analytes. DA, UA, and Trp contain aromatic rings in their molecular structures (Fig. 3c). Graphene nanosheets have strong adsorption affinities to aromatic rings because strong π - π interactions between the free π -bonds of sp^2 atoms from the six-benzene-ring graphene and the aromatic rings from DA, UA, and Trp. Hence, high oxidation currents translate to higher sensitivity in the detection of DA, UA, and Trp than in the detection of AA and NO₂⁻.

Due to the availability of both large peak separations and enhanced currents, the graphene/Ta wire electrode is the best electrode for sensing the simultaneous detection of AA, DA, UA, Trp, and NO₂⁻. Freestanding graphene nanosheets are exposed to a lot of edges defects (Raman spectrum in Fig. 1f) and to the active sites from edge defects of graphene^{53–55}.

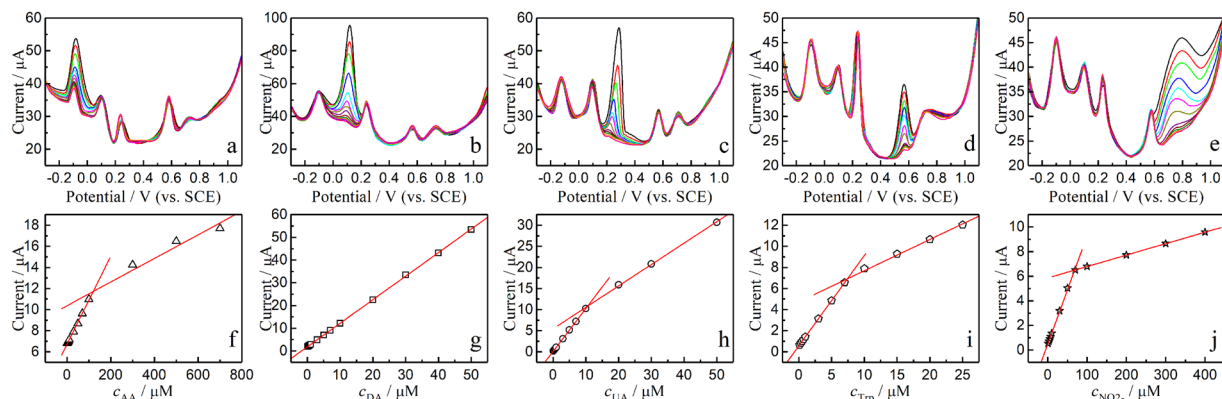


Figure 4. (a–e) DPVs of the graphene/Ta wire electrode for selective determination of AA, DA, UA, Trp, and NO₂⁻ in pH 7.0 PBS solution. (f–j) The plots of the oxidation peak currents versus variation in the concentrations.

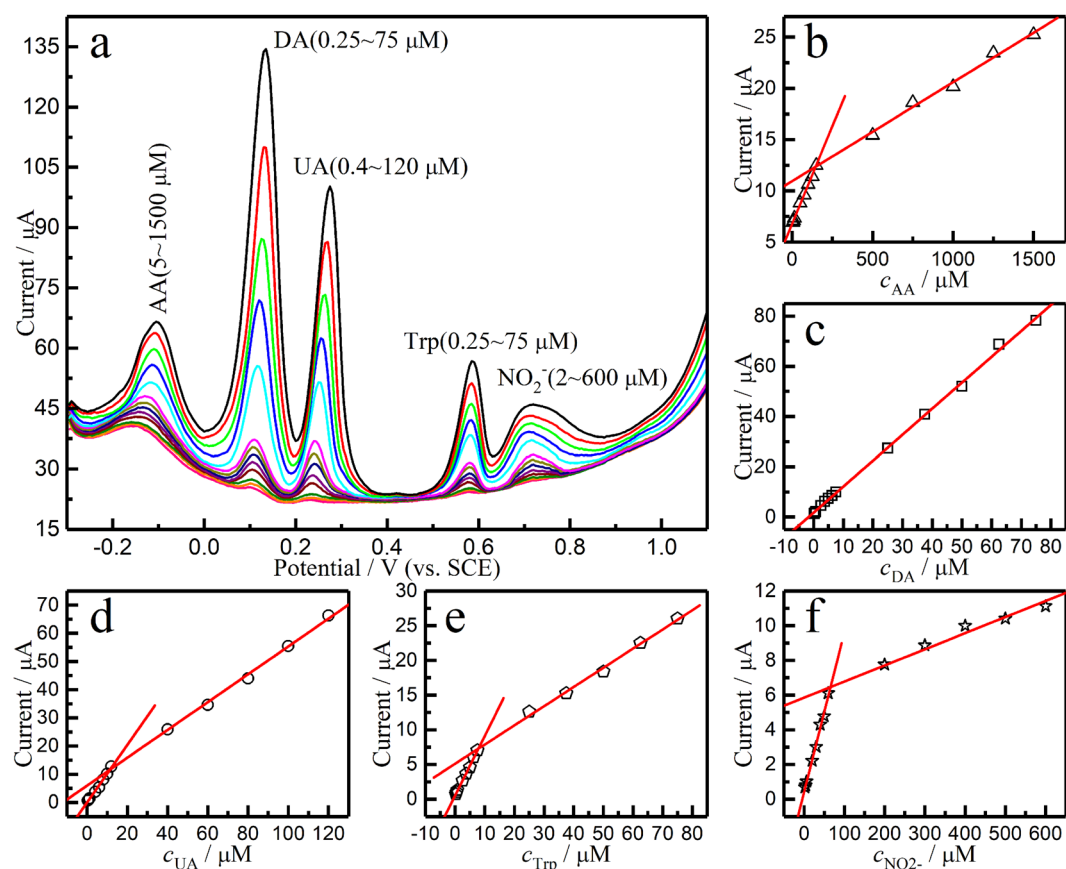


Figure 5. (a) DPV curves of graphene/Ta wire electrode in 0.1 M PBS (pH 7.0) with various concentrations of AA, DA, UA, Trp, and NO₂⁻. (b–f) Plots show peak currents versus the concentrations of AA, DA, UA, Trp, and NO₂⁻, respectively.

Determination of five species. Because pH has a profound effect on the electrochemical response of the sensing electrodes toward the simultaneous determination of AA, DA, UA, Trp, and NO₂⁻, the dependence of the peak potentials and currents of these five species oxidation on the different pH are shown in Fig. S3. In order to optimize sensitivity, selectivity, and practicability, pH 7.0 was selected for further experiments based on the results of the experiment shown in Fig. S3.

In order to identify the key parameters for detection of five species at graphene/Ta wire as a biosensor, the DPV curves of the mixtures of AA, DA, UA, Trp, and NO₂⁻ with various concentrations are measured selectively and simultaneously, as shown in Figs 4 and 5. Selective detection of five species showed the concentrations of four species to remain unchanged. Only one analyte showed any difference in concentration of one analyte. As shown

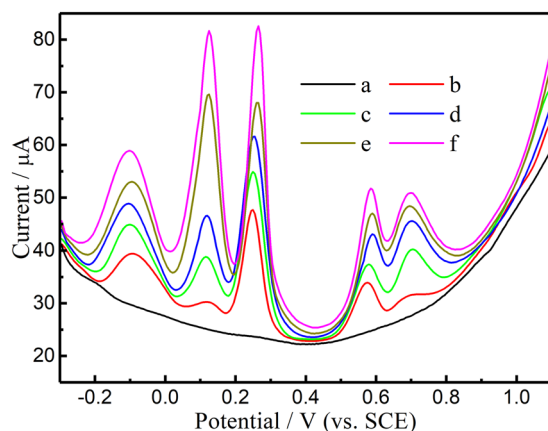


Figure 6. DPV curves of the graphene/Ta wire electrode in PBS the (a) absence and (b) presence of human serum and in (c–f) human serum containing additional AA, DA, UA, Trp, and NO_2^- .

in Figs 4 and 5, the peak currents were directly proportional to the concentrations of AA, DA, UA, Trp, and NO_2^- . The concentration range, regression equation, and detection limit (LOD) are summarized in Table S1.

When the five analytes were detected simultaneously, i.e. when the concentrations of all five were changed, the calibration curves were linear and within the concentration ranges of 5–1500 μM for AA, 0.25–75 μM for DA, 0.4–120 μM for UA, 0.25–75 μM for Trp, and 2–600 μM for NO_2^- . The slopes of the working curves changed at certain concentrations for AA, UA, Trp, and NO_2^- . H. Y. *et al.* explained the phenomenon with the change of adsorption interaction⁴⁹. The interface interaction of monolayer adsorption is strong, while that of multilayer adsorption is weak; hence, the slope of the working curve changed with increase in the concentration of analytes. Further, since the DA molecule contains an aromatic ring, a well-ordered organic layer was formed between the graphene and the aromatic ring of DA through π - π stacking interactions, which resulted in strong adsorption; therefore, the slope did not change within this concentration range. Compared with the flat graphene composite electrode, the sensitivity of the graphene/Ta wire electrode reached the same level, and the detection limits of DA, UA, and Trp are very advantageous^{5, 26, 56}.

The LOD for AA, DA, UA, Trp, and NO_2^- was found to be 1.58, 0.06, 0.09, 0.10, and 6.45 μM , respectively. The lowest LODs obtained here for simultaneous determination of AA, DA, UA, Trp, and NO_2^- were comparable to or in some cases better than previously reported values. In Table S3, some of the analytical characteristics obtained in this work were compared to values previously reported in the literature^{5, 21, 49, 56–59}. All this evidence supports the idea that the graphene/Ta wire electrode has an excellent ability to determine AA, DA, UA, Trp, and NO_2^- .

The stability of the graphene/Ta wire electrode was also studied in this work. When the electrode was cyclically swept for 100 cycles, there was a 4.8% decrease in the initial response of the graphene electrode, indicating that the graphene electrode had excellent stability (Fig. S4). The reproducibility of the graphene electrode was determined using six different electrodes. The relative standard deviations (RSD) of the current responses for AA, DA, UA, Trp, and NO_2^- were 3.4%, 5%, 4%, 5%, and 4.5%, respectively.

Several forms of inorganic, organic, and biological interference were tested to determine whether they could affect the detection of AA, DA, UA, Trp, and NO_2^- . These interferences were investigated at various concentrations in 0.1 M PBS (pH 7.0) containing 500 μM AA, 25 μM DA, 40 μM UA, 25 μM Trp, and 200 μM NO_2^- (Fig. S5). The results showed that concentrations of 500 μM CaCl_2 , 500 μM CuSO_4 , 500 μM KCl, 500 μM $\text{Mg}(\text{NO}_3)_2$, 500 μM $\text{Ni}(\text{NO}_3)_2$, 500 μM $\text{Zn}(\text{NO}_3)_2$, 500 μM Na_2S , 500 μM FeSO_4 , 25 μM aniline, 25 μM phenol, 25 μM hydroquinone, 25 μM catechol, 25 μM resorcinol, 25 μM citric acid, 25 μM glucose, 25 μM L-alanine, 25 μM L-cysteine, 25 μM L-glycine, 25 μM L-lysine, and 25 μM L-tyrosine did not significantly influence the height of the peak currents. The tolerance limit was defined as the concentration giving an error of $\leq 5\%$ in the determination of AA, DA, UA, Trp, and NO_2^- compounds. These results strongly demonstrate that the as-prepared graphene/Ta wire electrode performs with high selectivity and involves little interference.

Real sample analysis. To evaluate the application of the graphene/Ta wire electrode, an attempt was made to detect five species in the human serum samples. Each sample was diluted 5 times with 0.1 M PBS (pH 7.0) before measurement. The electrochemical responses for detection of AA, DA, UA, Trp, and NO_2^- as shown in Fig. 6. The analytical results are presented in Table S4. The recovery was in the range of 94–104% for all analytes. We compared the results of various methods for the determination of concentration of the five analytes in serum (Table S5). In general, the concentrations of AA, DA, UA, and Trp are closer to those obtained by CL⁶⁰, HPLC-CL⁶¹, GC/MS⁶², and UV methods⁶³; however, the concentration of NO_2^- is significantly higher than that measured by the spectrophotometric methods in the ref. 64. Since the sensitivities of various detection methods are different, and so are the serum samples, the results vary. However, the results show the presence of these substances in human serum. These results indicated that graphene/Ta wire could produce results accurate enough for clinical diagnosis.

Conclusions

Free-standing graphene nanosheets were here fabricated on Ta wire, which was used to selectively and simultaneously detect AA, DA, UA, Trp, and NO_2^- using a DPV method. The graphene electrode provided highly selective, sensitive results, with detection limits of AA, DA, UA, Trp, and NO_2^- of 1.58, 0.06, 0.09, 0.10, and 6.45 μM ($S/N = 3$), respectively. The key features of the graphene electrode responsible for its sensitivity improvement were found to be as follows: (i) free-standing nanosheets interlaced to form a network with mesoporous structures, which increased the surface area of the electrode, thereby facilitating ion adsorption on the surface of the electrode; (ii) high conductivity from CVD graphene nanosheets accelerated the ion diffusion and electron transfer. Free-standing graphene nanosheets are exposed to a lot of edges defects and to the active sites from edge defects of graphene. The Fermi level of graphene, HOMO, and LUMO of analytes affected the oxidation potential of the analytes. The two factors endowed the graphene electrode with high selectivity.

Methods

Reagents and materials. AA and DA were purchased from Aladdin Reagent Co., Ltd. (Shanghai, China). UA was purchased from Sigma Aldrich (U.S.). Trp and sodium nitrite (NaNO_2) were purchased from Tianjin Guangfu Fine Chemical Research Institute (Tianjin, China). Phosphate buffered solutions (PBS) with various pH values were prepared using 0.1 M Na_2HPO_4 and 0.1 M NaH_2PO_4 . Ultra-pure water was used in all experiments.

Preparation of graphene. Ta wires with a diameter of 0.6 mm were cut from 5 cm length wire-like substrates. The free-standing graphene nanosheets covered Ta wires, i.e. the graphene/Ta wire electrodes were prepared using a high-power direct current (DC) arc plasma jet CVD operating at gas recycling mode. The Ta wires were cleaned and attached to catalysts as follows before being placed in the deposition chamber: ultrasonic cleaning in ethanol and ultra-pure water, drying, immersion in the catalyst precursor solution (0.6 M $\text{Ni}(\text{NO}_3)_2$), and drying. The main deposition parameters are shown in Table S2.

Characterization. The morphology of the CVD graphene obtained by scanning electron microscopy (SEM; Carl Zeiss MERLIN Compact, Germany), transmission electron microscopy (TEM; JEOL JEM-2100, Japan) and atomic force microscopy (AFM; Agilent 5500, U.S.) measurements, respectively. Sample treatment for AFM measurement: The graphene/Ta wire electrode was immersed in ethanol and sonicated in an ultrasonic bath for 48 h (600 W/40 kHz). During this time, a small amount of graphene sheet was peeled off and dispersed in ethanol. The graphene/ethanol solution was then sprayed onto the Si wafer and dried. The Raman spectrum of graphene was recorded on a Renishaw Raman microscope with an excitation laser wavelength at 532 nm. X-ray diffraction (XRD) spectra were created using a Rigaku Ultima IV x-ray diffractometer with CuK_α radiation (wavelength of 0.15406 nm).

The electrochemical performance was investigated using cyclic voltammetry (CV), differential pulse voltammetry (DPV), and electrochemical impedance spectroscopy (EIS) with a CHI 660E electrochemical workstation (Shanghai Chenhua Instrument Co., Ltd.). In a three-electrode system, a graphene/Ta wire electrode/or other sample electrodes, a platinum (Pt) sheet and a saturated calomel electrode (SCE) served as the working electrode, counter electrode, and reference electrode, respectively (Fig. 1a).

References

- Zhou, Y. *et al.* Fabrication of electrochemical interface based on boronic acid-modified pyrroloquinoline quinone/reduced graphene oxide composites for voltammetric determination of glycosylated hemoglobin. *Biosens. Bioelectron.* **64**, 442–448 (2015).
- Viswambhari Devi, R., Doble, M. & Verma, R. S. Nanomaterials for early detection of cancer biomarker with special emphasis on gold nanoparticles in immunoassays/sensors. *Biosens. Bioelectron.* **68**, 688–698 (2015).
- Pramanick, B. *et al.* Human hair-derived hollow carbon microfibers for electrochemical sensing. *Carbon* **107**, 872–877 (2016).
- Arvand, M. & Dehsaraei, M. A simple and efficient electrochemical sensor for folic acid determination in human blood plasma based on gold nanoparticles-modified carbon paste electrode. *Mater. Sci. Eng., C* **33**, 3474–3480 (2013).
- Yang, Y. J. & Li, W. K. CTAB functionalized graphene oxide/multiwalled carbon nanotube composite modified electrode for the simultaneous determination of ascorbic acid, dopamine, uric acid and nitrite. *Biosens. Bioelectron.* **56**, 300–306 (2014).
- Reddaiah, K., Reddy, M. M., Raghu, P. & Reddy, T. M. An electrochemical sensor based on poly (solochrome dark blue) film coated electrode for the determination of dopamine and simultaneous separation in the presence of uric acid and ascorbic acid: A voltammetric method. *Colloids Surf., B* **106**, 145–150 (2013).
- He, H., Xu, X., Wang, P., Chen, L. & Jin, Y. The facile surface chemical modification of a single glass nanopore and its use in the nonenzymatic detection of uric acid. *Chem. Commun.* **51**, 1914–1917 (2015).
- Abraham, A. & Drory, V. E. Influence of serum uric acid levels on prognosis and survival in amyotrophic lateral sclerosis: a meta-analysis. *J. Neurol.* **261**, 1133–1138 (2014).
- Özcan, A. & Şahin, Y. A novel approach for the selective determination of tryptophan in blood serum in the presence of tyrosine based on the electrochemical reduction of oxidation product of tryptophan formed *in situ* on graphite electrode. *Biosens. Bioelectron.* **31**, 26–31 (2012).
- Canbay, E., Şahin, B., Kıran, M. & Akyılmaz, E. MWCNT–cysteamine–Nafion modified gold electrode based on myoglobin for determination of hydrogen peroxide and nitrite. *Bioelectrochemistry* **101**, 126–131 (2015).
- Menart, E., Jovanovski, V. & Hočevar, S. B. Silver particle-decorated carbon paste electrode based on ionic liquid for improved determination of nitrite. *Electrochem. Commun.* **52**, 45–48 (2015).
- Ahn, J.-H., Jo, K. H. & Hahn, J. H. Standard addition/absorption detection microfluidic system for salt error-free nitrite determination. *Anal. Chim. Acta* **886**, 114–122 (2015).
- Ramakrishnan, S. *et al.* One-step synthesis of Pt-decorated graphene-carbon nanotubes for the electrochemical sensing of dopamine, uric acid and ascorbic acid. *Anal. Methods* **7**, 779–786 (2015).
- Qi, S., Zhao, B., Tang, H. & Jiang, X. Determination of ascorbic acid, dopamine, and uric acid by a novel electrochemical sensor based on pristine graphene. *Electrochim. Acta* **161**, 395–402 (2015).
- Chen, L.-X. *et al.* Facile synthesis of porous bimetallic alloyed PdAg nanoflowers supported on reduced graphene oxide for simultaneous detection of ascorbic acid, dopamine, and uric acid. *Analyst* **140**, 3183–3192 (2015).

16. Imran, H., Manikandan, P. N. & Dharuman, V. Facile and green synthesis of graphene oxide by electrical exfoliation of pencil graphite and gold nanoparticle for non-enzymatic simultaneous sensing of ascorbic acid, dopamine and uric acid. *RSC Adv.* **5**, 63513–63520 (2015).
17. Zhao, L. *et al.* MgO nanobelt-modified graphene-tantalum wire electrode for the simultaneous determination of ascorbic acid, dopamine and uric acid. *Electrochim. Acta* **168**, 191–198 (2015).
18. Ghoreishi, S. M., Behpour, M., Mousavi, S., Khoobi, A. & Ghoreishi, F. S. Designing a nanostructure-based modified electrode as a biosensor for simultaneous determination of tryptophan and uric acid. *Anal. Methods* **7**, 466–471 (2015).
19. Li, Y., Li, J., Shanguan, E. & Li, Q. The effect of acidity, hydrogen bond catalysis and auxiliary electrode reaction on the oxidation peak current for dopamine, uric acid and tryptophan. *Anal. Methods* **7**, 2636–2644 (2015).
20. Noroozifar, M., Khorasani-Motlagh, M., Hassani Nadiki, H., Saeed Hadavi, M. & Mehdi Foroughi, M. Modified fluorine-doped tin oxide electrode with inorganic ruthenium red dye-multiwalled carbon nanotubes for simultaneous determination of a dopamine, uric acid, and tryptophan. *Sens. Actuators, B* **204**, 333–341 (2014).
21. Kaur, B., Satpati, B. & Srivastava, R. Synthesis of NiCo₂O₄/Nano-ZSM-5 nanocomposite material with enhanced electrochemical properties for the simultaneous determination of ascorbic acid, dopamine, uric acid and tryptophan. *New J. Chem.* **39**, 1115–1124 (2015).
22. Prathap, M. U. A. & Srivastava, R. Tailoring properties of polyaniline for simultaneous determination of a quaternary mixture of ascorbic acid, dopamine, uric acid, and tryptophan. *Sens. Actuators, B* **177**, 239–250 (2013).
23. Azzouzi, S. *et al.* A novel amperometric biosensor based on gold nanoparticles anchored on reduced graphene oxide for sensitive detection of l-lactate tumor biomarker. *Biosens. Bioelectron.* **69**, 280–286 (2015).
24. Pruneanu, S. *et al.* The influence of uric and ascorbic acid on the electrochemical detection of dopamine using graphene-modified electrodes. *Electrochim. Acta* **154**, 197–204 (2015).
25. Jiang, J. J., Fan, W. J. & Du, X. Z. Nitrite electrochemical biosensing based on coupled graphene and gold nanoparticles. *Biosens. Bioelectron.* **51**, 343–348 (2014).
26. Yang, Y. J. One-pot synthesis of reduced graphene oxide/zinc sulfide nanocomposite at room temperature for simultaneous determination of ascorbic acid, dopamine and uric acid. *Sens. Actuators, B* **221**, 750–759 (2015).
27. Palanisamy, S. *et al.* A Facile Electrochemical Preparation of Reduced Graphene Oxide@Polydopamine Composite: A Novel Electrochemical Sensing Platform for Amperometric Detection of Chlorpromazine. *Sci. Rep.* **6**, 33599 (2016).
28. Raj, M., Gupta, P., Goyal, R. N. & Shim, Y. B. Graphene/conducting polymer nano-composite loaded screen printed carbon sensor for simultaneous determination of dopamine and 5-hydroxytryptamine. *Sens. Actuators, B* **239**, 993–1002 (2017).
29. Song, H. *et al.* Simultaneous voltammetric determination of dopamine and uric acid using carbon-encapsulated hollow Fe₃O₄ nanoparticles anchored to an electrode modified with nanosheets of reduced graphene oxide. *Microchim. Acta* **184**, 843–853 (2017).
30. Chen, Y. L. *et al.* 8-aminoquinoline functionalized graphene oxide for simultaneous determination of guanine and adenine. *J. Solid State Electrochem.* **21**, 1357–1364 (2017).
31. Tig, G. A., Gunendi, G. & Pekyardimci, S. A selective sensor based on Au nanoparticles-graphene oxide-poly(2,6-pyridinedicarboxylic acid) composite for simultaneous electrochemical determination of ascorbic acid, dopamine, and uric acid. *J. Appl. Electrochem.* **47**, 607–618 (2017).
32. Zhang, D., Li, L., Ma, W., Chen, X. & Zhang, Y. Electrodeposited reduced graphene oxide incorporating polymerization of l-lysine on electrode surface and its application in simultaneous electrochemical determination of ascorbic acid, dopamine and uric acid. *Mater. Sci. Eng., C* **70**, Part 1, 241–249 (2017).
33. Abdelwahab, A. A. & Shim, Y.-B. Simultaneous determination of ascorbic acid, dopamine, uric acid and folic acid based on activated graphene/MWCNT nanocomposite loaded Au nanoclusters. *Sens. Actuators, B* **221**, 659–665 (2015).
34. Yokuş, Ö. A. *et al.* Sensitive voltammetric sensor based on polyoxometalate/reduced graphene oxide nanomaterial: Application to the simultaneous determination of l-tyrosine and l-tryptophan. *Sens. Actuators, B* **233**, 47–54 (2016).
35. Nguyen, D. D. *et al.* Macroscopic, freestanding, and tubular graphene architectures fabricated via thermal annealing. *ACS Nano* **9**, 3206–3214 (2015).
36. Kim, H., Park, J.-H., Suh, M., Real Ahn, J. & Ju, S. Horizontally aligned ZnO nanowire transistors using patterned graphene thin films. *Appl. Phys. Lett.* **100**, 063112 (2012).
37. Jang, J. *et al.* Low-temperature-grown continuous graphene films from benzene by chemical vapor deposition at ambient pressure. *Sci. Rep.* **5**, 17955 (2015).
38. Yue, H. Y. *et al.* Synthesis of ZnO nanowire arrays/3D graphene foam and application for determination of levodopa in the presence of uric acid. *Biosens. Bioelectron.* **89**, 592–597 (2017).
39. Shackery, I. *et al.* Sensitivity Enhancement in Nickel Hydroxide/3D-Graphene as Enzymeless Glucose Detection. *Electroanalysis* **27**, 2363–2370 (2015).
40. Osikoya, A. O. *et al.* Acetylene-sourced CVD-synthesised catalytically active graphene for electrochemical biosensing. *Biosens. Bioelectron.* **89**, 496–504 (2017).
41. Zhong, Z. *et al.* Signal-on electrochemical immunoassay for APE1 using ionic liquid doped Au nanoparticle/graphene as a nanocarrier and alkaline phosphatase as enhancer. *Analyst* **139**, 6563–6568 (2014).
42. Cazetta, A. L. *et al.* NaOH-activated carbon of high surface area produced from coconut shell: Kinetics and equilibrium studies from the methylene blue adsorption. *Chem. Eng. J.* **174**, 117–125 (2011).
43. Quinlan, R. A. *et al.* Investigation of defects generated in vertically oriented graphene. *Carbon* **64**, 92–100 (2013).
44. Takahashi, T., Sugawara, K., Noguchi, E., Sato, T. & Takahashi, T. Band-gap tuning of monolayer graphene by oxygen adsorption. *Carbon* **73**, 141–145 (2014).
45. Wakabayashi, K., Takane, Y., Yamamoto, M. & Sigrist, M. Edge effect on electronic transport properties of graphene nanoribbons and presence of perfectly conducting channel. *Carbon* **47**, 124–137 (2009).
46. Ge, C. *et al.* Synthesis of a ZnO nanorod/CVD graphene composite for simultaneous sensing of dihydroxybenzene isomers. *Carbon* **95**, 1–9 (2015).
47. Davami, K. *et al.* Synthesis and characterization of carbon nanowalls on different substrates by radio frequency plasma enhanced chemical vapor deposition. *Carbon* **72**, 372–380 (2014).
48. Neumann, C. *et al.* Raman spectroscopy as probe of nanometre-scale strain variations in graphene. *Nat. Commun.* **6**, 8429 (2015).
49. Yue, H. Y. *et al.* ZnO Nanowire Arrays on 3D Hierarchical Graphene Foam: Biomarker Detection of Parkinson's Disease. *ACS Nano* **8**, 1639–1646 (2014).
50. Lin, Y.-J. & Zeng, J.-J. Determination of Schottky barrier heights and Fermi-level unpinning at the graphene/n-type Si interfaces by X-ray photoelectron spectroscopy and Kelvin probe. *Appl. Surf. Sci.* **322**, 225–229 (2014).
51. Shukla, M. K. & Mishra, P. C. Electronic structures and spectra of two antioxidants: uric acid and ascorbic acid. *J. Mol. Struct.* **377**, 247–259 (1996).
52. Mohammad-Shiri, H., Ghaemi, M., Riahi, S. & Akbari-Sehat, A. Computational and Electrochemical Studies on the Redox Reaction of Dopamine in Aqueous Solution. *Int. J. Electrochem. Sci.* **6**, 317–336 (2011).
53. Deng, K.-Q., Zhou, J.-h & Li, X.-F. Direct electrochemical reduction of graphene oxide and its application to determination of l-tryptophan and l-tyrosine. *Colloids Surf., B* **101**, 183–188 (2013).
54. Mota Ferreira, G. M. *et al.* DNA and graphene as a new efficient platform for entrapment of methylene blue (MB): Studies of the electrocatalytic oxidation of beta-nicotinamide adenine dinucleotide. *Electrochim. Acta* **111**, 543–551 (2013).

55. Banhart, F., Kotakoski, J. & Krasheninnikov, A. V. Structural Defects in Graphene. *ACS Nano* **5**, 26–41 (2011).
56. Kaur, B., Pandiyan, T., Satpati, B. & Srivastava, R. Simultaneous and sensitive determination of ascorbic acid, dopamine, uric acid, and tryptophan with silver nanoparticles-decorated reduced graphene oxide modified electrode. *Colloids Surf., B* **111**, 97–106 (2013).
57. Wang, C. *et al.* Cu-nanoparticles incorporated overoxidized-poly (3-amino-5-mercapto-1,2,4-triazole) film modified electrode for the simultaneous determination of ascorbic acid, dopamine, uric acid and tryptophan. *J. Electroanal. Chem.* **741**, 36–41 (2015).
58. Li, S.-M. *et al.* Fabrication of a silver nanowire-reduced graphene oxide-based electrochemical biosensor and its enhanced sensitivity in the simultaneous determination of ascorbic acid, dopamine, and uric acid. *J. Mater. Chem. C* **3**, 9444–9453 (2015).
59. Sun, J. *et al.* Simultaneous determination of ascorbic acid, dopamine and uric acid at a nitrogen-doped carbon nanofiber modified electrode. *RSC Adv.* **5**, 11925–11932 (2015).
60. Chen, H., Li, R., Lin, L., Guo, G. & Lin, J.-M. Determination of L-ascorbic acid in human serum by chemiluminescence based on hydrogen peroxide-sodium hydrogen carbonate-CdSe/CdS quantum dots system. *Talanta* **81**, 1688–1696 (2010).
61. Chen, F.-N., Zhang, Y.-X. & Zhang, Z.-J. Simultaneous determination of epinephrine, noradrenaline and dopamine in human serum samples by high performance liquid chromatography with chemiluminescence detection. *Chin. J. Chem.* **25**, 942–946 (2007).
62. Sun, Y.-p., Chen, J., Qi, H.-y. & Shi, Y.-p. Graphitic carbon nitrides modified hollow fiber solid phase microextraction for extraction and determination of uric acid in urine and serum coupled with gas chromatography-mass spectrometry. *J. Chromatogr. B* **1004**, 53–59 (2015).
63. Miyado, T. *et al.* Development of a novel running buffer for the simultaneous determination of nitrate and nitrite in human serum by capillary zone electrophoresis. *J. Chromatogr. A* **1014**, 197–202 (2003).
64. Sastry, K. V. H., Moudgal, R. P., Mohan, J., Tyagi, J. S. & Rao, G. S. Spectrophotometric determination of serum nitrite and nitrate by copper-cadmium alloy. *Anal. Biochem.* **306**, 79–82 (2002).

Acknowledgements

This work was supported by the National Nature Science Foundation of China (Nos 61401306, 61301045, and 61504096), the National key R&D program of China (No. 2016YFB0402703), the Natural Science Foundation of Tianjin City (Nos 17JCZDJC32600, 15JCYBJC24000 and 16JCYBJC16300), and the Youth Top-Notch Talents Program of Tianjin.

Author Contributions

H.L. and M.L. conceived the experiments, X.W., D.G. and X.W. conducted the experiments, B.Y. analysed the results. All authors discussed the results and commented on the manuscript.

Additional Information

Supplementary information accompanies this paper at doi:10.1038/s41598-017-07646-2

Competing Interests: The authors declare that they have no competing interests.

Publisher's note: Springer Nature remains neutral with regard to jurisdictional claims in published maps and institutional affiliations.



Open Access This article is licensed under a Creative Commons Attribution 4.0 International License, which permits use, sharing, adaptation, distribution and reproduction in any medium or format, as long as you give appropriate credit to the original author(s) and the source, provide a link to the Creative Commons license, and indicate if changes were made. The images or other third party material in this article are included in the article's Creative Commons license, unless indicated otherwise in a credit line to the material. If material is not included in the article's Creative Commons license and your intended use is not permitted by statutory regulation or exceeds the permitted use, you will need to obtain permission directly from the copyright holder. To view a copy of this license, visit <http://creativecommons.org/licenses/by/4.0/>.

© The Author(s) 2017